Chandra Observations of Relativistic AGN Jets

D. A. Schwartz
Smithsonian Astrophysical Observatory, Cambridge, MA 02138, USA

We review Chandra observations of arcsecond scale radio jets in quasars and powerful FR II radio galaxies. The spatial correlation of X-ray and radio brightness clearly indicates a common origin, but detailed differences are significant. The radio/optical/X-ray spectral energy distributions typically do not allow a simple synchrotron model to produce the entire radiation spectrum. Assuming minimum energy density, we can explain the X-ray emission as inverse Compton scattering on the cosmic microwave background (CMB), and deduce that the jets are moving with bulk Lorentz factors of 3–12 on scales 100's of kpc from the central quasar. The power carried by these jets implies they play a critical role in the accretion onto the central black hole, and have a profound influence on their environment; e.g., by retarding cooling flows in clusters of galaxies. If inverse Compton scattering on the microwave background is producing X-rays in nearby jets such as PKS 0637-752, then intrinsically similar objects must be seen with the same surface brightness at whatever redshifts they exist.

1. INTRODUCTION

Prior to the launch of the *Chandra* X-ray Observatory [1] there were three significant detections of extragalactic X-ray jets [2]: in Cen A [3], in M87 [4], and in 3C 273 [5, 6]. Now X-ray observations of jets are contributing to a variety of problems, including the interaction with gas in Seyfert galaxies [7] and clusters of galaxies [8, 9]; hot-spots at the ends of jets [10, 11], jets in BL Lac objects [12] and FR I radio galaxies [13]; and the relativistic jets in quasars and powerful FR II radio sources [14, 15]. These studies are enabled by the magnificent angular resolution of the *Chandra* X-ray telescope, which results in a system resolution of about $0.77''$ full-width at half-maximum response. The 10-fold improvement in angular resolution with the *Chandra* X-ray telescope gives a 100-fold increase in spatial information, and enables resolution of faint surface brightness features near bright point sources (see Figure 1).

The present review will cover only the last topic: Relativistic jets in powerful active galactic nuclei (AGN). Historically, jets are a radio astronomy phenomena. The were theoretically motivated prior to being observed [16], in order to explain how large quantities of energy were transported to the lobes of giant radio galaxies. It is apparent that they are a significant part of the energy budget of the AGN's central black hole [17], and they must be interacting with the gas of their host galaxy, and with the intra-cluster medium when they occur in a cluster of galaxies. It is hoped that study of jets can tell us about the acceleration of the radiating electrons, and whether charge neutrality is maintained by positrons or by protons. There is also the question of how such powerful jets are accelerated and collimated by the central black hole. The broad band spectral energy distribution (SED) provided by the X-ray data allows a more complete picture of the radiation mechanisms operating in the jets. Since radiation observed in a given band arises primarily from electrons, (including positrons), within a distinct energy band, the lifetimes for particles which produce the different observed bands can be quite different, so that the spatial profiles will be telling us about the acceleration sites.

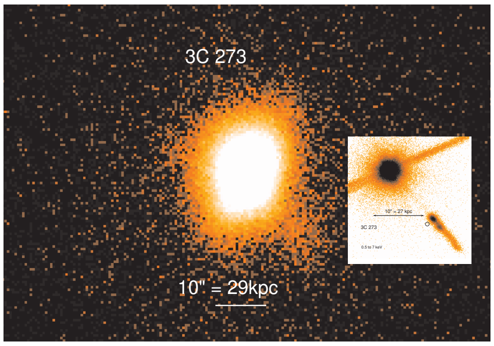

Figure 1: X-ray images of the quasar and jet of 3C 273 as observed by *ROSAT*, (left), and *Chandra*, right. Images are to the same scale and of comparable sensitivity. The jet image is only 0.1% of the intensity of the quasar core.

In this talk I present arguments for interpreting the X-ray emission as inverse Compton (IC) scattering off the cosmic microwave background (CMB) radiation. These arguments are based on the broad-band SED, on the ratio of X-ray to radio flux profiles, and on considering the relative energy densities in the magnetic field and CMB under the assumption of near minimum energy conditions. The IC/CMB interpretation allows us to estimate the magnetic field in the jet rest frame, the bulk Lorentz factor of the relativistic jet, and the minimum energy of the relativistic electrons in the jet. The most remarkable prediction of the IC/CMB scenario may be that such X-ray jets will be seen to very large redshifts [18], and may be detectable in γ-rays up to 100 MeV. This signature may ultimately distinguish the IC/CMB mechanism from alternate explanations in which the X-ray emission arises as synchrotron radiation [19–21].

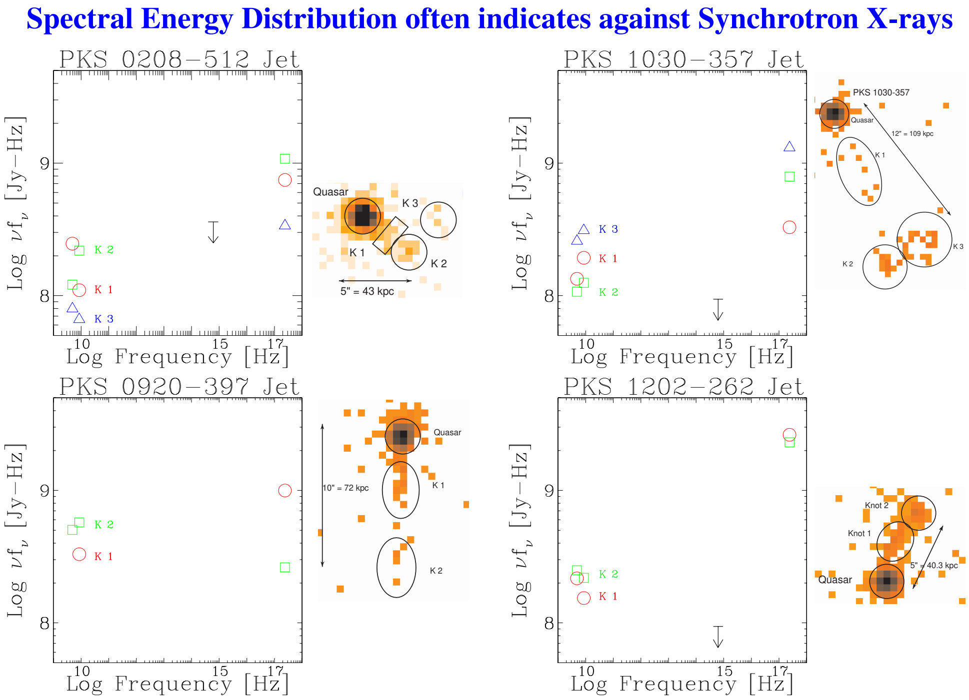

Figure 2: Spatially resolved SED for four jets observed in the Marshall [15] survey. The circles, squares, and triangles represent regions which are progressively further from the quasar, as indicated by the X-ray images to the right of each spectral plot. In the images, the X-rays are raw counts in the 0.5 to 7 keV band, binned in 0.5$''$ pixels. The faintest color is one single count, while the darkest regions are the quasar cores. The optical upper limits [27] for three of these prohibit explanation of the X-rays as a simple extrapolation of the radio synchrotron spectrum.

2. SPECTRAL ENERGY DISTRIBUTION

2.1. Inverse Compton Emission

The original *Chandra* observations of the jet of PKS 0637-752 noted that optical detection of the jet from the Hubble Space Telescope (HST) was at such a low flux density that the radio synchrotron spectrum could not be extrapolated to explain the X-ray emission as an extension of that synchrotron emission [22–24]. This led to the explanation of the X-rays as IC/CMB, with the additional assumption that the jet was in bulk relativistic motion [25, 26]. Such relativistic motion is generally inferred for the one-sided jets, even on scales of 10's of kpc, to explain the absence of the opposite jet via Doppler diminution.

For several of the quasar jets detected in short survey observations, there are sufficient data to construct spatially resolved radio/optical/X-ray SED. Figure 2 shows four such sources from the survey by Marshall et al. [15]. Each jet is resolved into 2 or 3 regions from which we measure flux densities at 4.8 and 8.6 GHz, and deduce an X-ray flux density at 1 keV (2.4 $\times$ 10^{17} Hz) by assuming a spectral shape $f_x \propto E^{-\alpha}$ where we take α=0.7. Optical measurements from Magellan [27], as well as the measured radio spectral index, prohibit explanation of the X-rays as an extension of the radio synchrotron at least in the cases of PKS 0208-512, PKS 1030-357, and PKS 1202-262.

In Figure 3, Sambruna et al. [14] have fit their GHz, HST, and X-ray measurements of the two brightest regions of four jets to radio synchrotron spectra, with a high energy cutoff, and IC/CMB from the same spectrum of electrons, with a low energy cutoff, to produce the X-ray emission. With the exception of knot A of 1136-135, we have further examples where the radio spectrum cannot be simply extrapolated to produce the X-rays via synchrotron emission. In cases such as 1136-135, 1150+497, and 1354+195, the synchrotron cutoff is at a high enough frequency that the IC/CMB emission should be extending up past the 100 Gev range, 10^{23} Hz. In this range, the *GLAST* satellite to be launched in 2007 is expected to be have a flux detection limit of 10^{-12} to 10^{-13} ergs cm^{-2} s^{-1}. It is possible that the large scale jets from these particular sources will be detected, especially if the spectral index is just slightly flatter than has been fit. Of course *GLAST* will not have the spatial resolution to distinguish the jet from the core, so the identification would need to be made on the basis of lack of time variability, and on extrapolation from an accurate spectral index measured in the X-ray band.

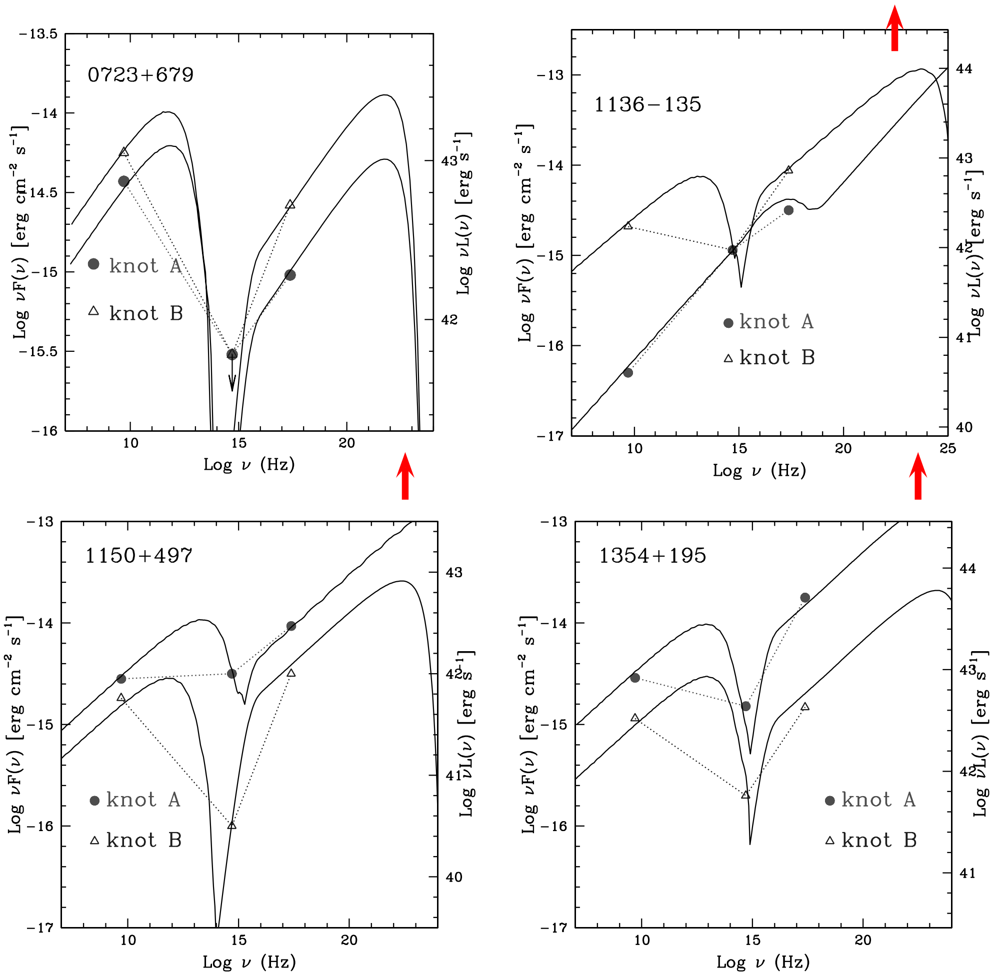

Figure 3: SED for four jets observed in the Sambruna [14] survey, fit to spectra with radio synchrotron emission and X-ray IC/CMB emission. The arrows show the approximate sensitivity limit for *GLAST* at $10^{22.5}$ Hz, which might detect the γ-ray emission from the 100 kpc scale jets. Taken from Figure 8 of Sambruna et al. [14].

2.2. Low Energy Electron Spectrum Cutoff

Figure 4 shows some preliminary work by Martin Mueller [28] to determine an upper limit to the low energy cutoff of the relativistic electrons. The plus signs show 78 ks data from the jet of PKS 0637-752, obtained during the initial on-orbit observations used to focus the *Chandra* Observatory. This data is especially useful since the ACIS filter was inferred to have very little contamination at that time. The solid histogram gives the X-ray spectrum predicted from IC/CMB, assuming an electron spectrum $N_e(\gamma) \propto \gamma^{-2.6}$, where the index is selected to match the observed ratio spectral index of 0.8. The low energy electron cutoff is schematically indicated by the exponential decrease below γ_{min}. For the curve shown γ_{min}=80, and this is marginally the highest allowed value statistically consistent with the measured data.

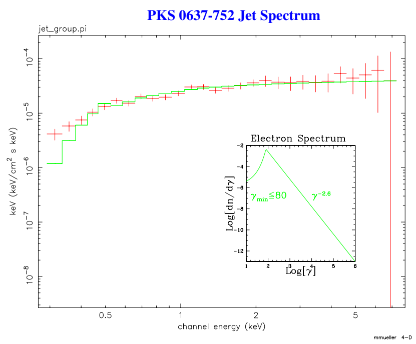

Figure 4: Upper limit to the low energy electron cutoff in the PKS 0637-752 jet. Data (plus signs) are 78 ks taken from the *Chandra* focusing operations. The solid line is a predicted spectrum with γ_{min}=80, so that higher values of γ_{min} would conflict with the observations. The insert shows the assumed relativistic electron spectrum.

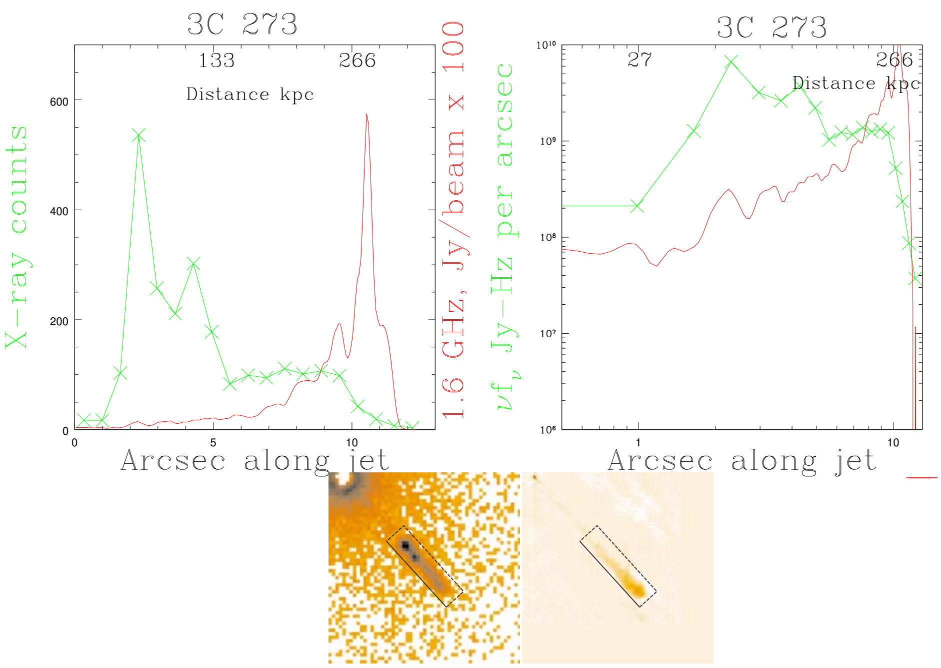

Figure 5: Radio and X-ray profiles along the jet of 3C 273. X-ray data is the line connecting crosses, radio data is the solid line. The upper left panel plots X-ray counts per bin, and 1.6 GHz flux density per beam, arbitrarily scaled. Upper right panel plots the radiated energy in each band, in Jy-Hz per arcsec. The small lower panels show false color images of the X-ray, left, and radio jet. The linear scale in kpc assumes the jet is at 0.1 radian to our line of sight.

3. X-RAY AND RADIO PROFILES

X-ray and radio surface brightness generally arise from the same region, and most probably both can be explained in the context of a single, self-consistent physical model of the jet. We see at least two distinct morphological patterns, each of which raises puzzles no matter what emission mechanism is invoked. In the quasar 3C 273, Figure 5, the X-ray emission decreases markedly while the 1.6 GHz radio emission increases moving along the jet away from the quasar. The upper left panel plots the total X-ray counts per bin marked by the “x’s” and the 1.6 GHz flux density in Jy/beam scaled by a factor of 100. The upper right hand panel shows the radiated energy, νf_ν in each band. Note that the X-rays dominate the radiated energy from the jet, a pattern which is typical in all the jets detected by *Chandra*. The projections are made along the solid lines in the two bottom figures, starting about 10″ from the quasar and integrating about 2″ perpendicular to the line of projection.

Marshall et al. [29] showed a general correlation of the X-ray features with the optical and radio knots [30]. In Figure 6 we compare the X-ray and radio profiles in more detail. Here we have used a total of 430 ks from calibration observations of 3C 273, primarily from the zero order image of transmission grating observations. We have scaled different angular segments of the radio profile by different factors to better compare with the X-ray profile. The ratio of X-ray to radio flux changes by a factor of 400 over the 11″length of the jet. While some regions show a

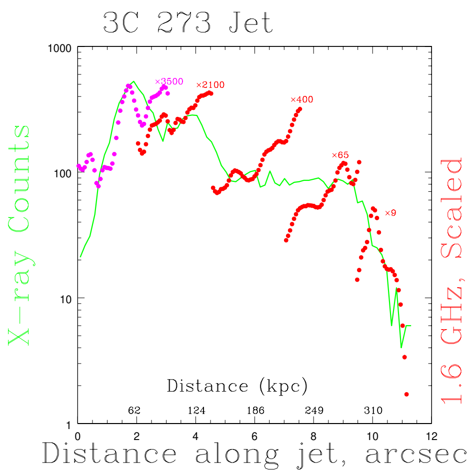

Figure 6: The projected X-ray profile is shown as a solid line, generally decreasing toward the end of the jet. The 1.6 GHz radio emission is shown as a series of segments (dotted) which are scaled by different factors to best compare with the X-ray emission from the same region.

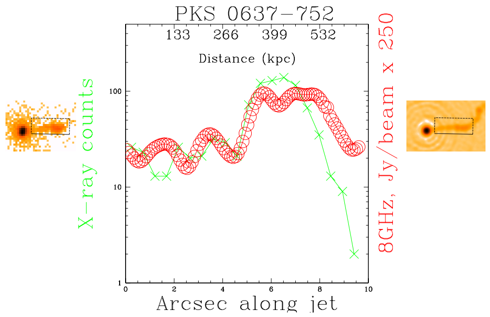

Figure 7: X-ray and radio profiles for PKS 0637-752, projected along the boxes shown in the small images to the left and right, respectively. The ordinate shows X-ray counts per bin, the solid line connecting the crosses, and the 8.6GHz radio flux density per beam in arbitrary units, circles. The de-projected distance is shown on the top axis.

very similar X-ray to radio behavior; e.g., from 1″ to 2″, 3″ to 4″, and 10.5″ to 11.5″, the region from 6″ to 9″ shows a constant X-ray emission while the radio increases more than a factor of 10.

Several other jets show a profile where the ratio of X-ray to radio brightness varies by no more than a factor of two for many arcseconds – corresponding to intrinsic lengths of several 100 kpc. Figure 7 shows the case of PKS 0637-752 [22, 24]. The boxes indicate the region of the projection. The ratio is quite constant out to about 8″ along the jet. At that point, the 8.6 GHz radio jet makes a large angle bend and the X-ray emission ceases.

Either of those two patterns is difficult to explain, no matter whether the X-rays are produced by synchrotron or by IC/CMB. In the IC/CMB case for 3C 273 we cannot explain why the X-rays decrease and the radio increases, since in this mechanism the X-rays are produced by lower energy electrons which have longer lifetimes and should persist further than the radio electrons. For PKS 0637-752 in the IC/CMB case, a constant f_x/f_r ratio can be explained as emission by a constant particle population, but then we require the magnetic field, which only influences the synchrotron radio emission, to be quite constant, even where the X-ray and radio emission increases by about a factor of 5 in the 4.5″ to 5.5″ region. In the case of synchrotron X-ray emission, the lifetimes of the X-ray emitting electrons is so short, of order years, that there should no relation at all between the X-ray and radio emission. In the IC/CMB scenario we know that relativistic beaming of the jet plays a role, and indeed such beaming was key to the original explanation of the X-ray emission in PKS 0637-752 [25, 26]. The resolution of these puzzles likely involves a physical connection among several variables or processes, including the magnetic field, acceleration of particles, and changes in the bulk velocity or direction of the jet. The filling factor, the fraction of the volume assumed

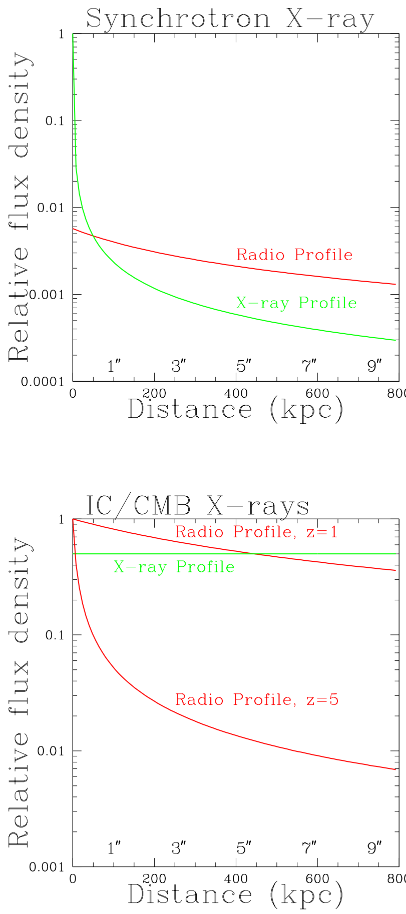

Figure 8: Toy models of synchrotron and IC/CMB profiles. These assume a jet at redshift z=1, with internal field B=10μG, bulk Lorentz factor Γ=10, at 5° from our line of sight. The electrons are assumed to be accelerated at the origin, and to produce radiation according to equations 1 and 2.

filled with a randomly oriented uniform magnetic field strength and uniform isotropic particle densities, may deviate from the value unity which is typically assumed. It is important to determine which mechanism dominates the jet X-ray production in order to better understand the internal structure.

In figure 8 we create very naive models of the radio and of the X-ray profiles for synchrotron and for IC/CMB emission. Following Felten and Morrison [31] we assume the radiation comes from electrons of a single energy $\gamma_\nu mc^2$, where the synchrotron radiation is at frequency in Hz:

$$\nu_s = 4.2\gamma_\nu^2 B \qquad (1)$$

and the IC/CMB radiation frequency is

$$\nu_{IC} = 7.5 \times 10^{10}\gamma_\nu^2 \mathrm{T}. \qquad (2)$$

We assume the electrons are accelerated at the start of the jet, which is moving with bulk velocity Γ=10 at an angle θ=5°. We assume the jet is at redshift z=1, and has an internal magnetic field B=10μGauss. Then the profile is taken as just the loss of electron energy dE/dt in ergs s^{-1} due to the rate of radiation: for synchrotron,

$$\frac{\mathrm{dE}}{\mathrm{dt}} = 1.6 \times 10^{-27} \gamma^2 B^2 \tag{3}$$

and for IC/CMB,

$$\frac{\mathrm{dE}}{\mathrm{dt}} = 2.6 \times 10^{-14} \gamma^2 \rho. \tag{4}$$

In the above equations, B is the perpendicular magnetic field in μGauss, $T=(1+z)T_0$ is the CMB temperature at redshift z, T_0=2.728 K [32], and $\rho = \Gamma^2 aT^4 = 7.56 \times 10^{-15}\, \Gamma^2\, T_0^4\, (1+z)^4$ is the CMB energy density as seen in the jet rest frame.

In any synchrotron X-ray scenario the lifetime of the electrons is so short that the X-ray emission detected by *Chandra* appears as an unresolved source at the location of acceleration, and there is no *a priori* relation to be expected between the X-ray and radio profile. However, in the case of IC/CMB, both the radio and X-ray profiles change rather gradually on the scales of $\approx 10''$ or 100's of kpc, which are typical of the *Chandra* jet observations. This qualitatively suggests the IC/CMB mechanism, although it does not address the issue restricting the magnetic field variation mentioned above. At high redshifts, e.g. z=5 as shown in Figure 8, the synchrotron emitting electrons become lifetime limited by their IC/CMB radiation, and we should predict that we would not find similar constancy of f_x/f_r as observed in sources at z$\lesssim$2.

This simplistic model fails the most basic prediction, which is that if the electrons are accelerated at discrete locations, the X-ray and radio peak intensities should always be coincident, with X-ray or radio surface brightness decreasing more rapidly depending whether synchrotron or IC/CMB, respectively, is dominating. However there are numerous cases of offsets in the peak emission. Most dramatic may be the case of PKS 1127-145 reported by Siemiginowska et al. [33] and shown in Figure 9.

Most likely, acceleration processes are occurring in many locations, if not continuously, along a jet. A complete, successful model of a jet must treat the entire observed jet as a single entity, and not only the discrete bright regions usually called "knots."

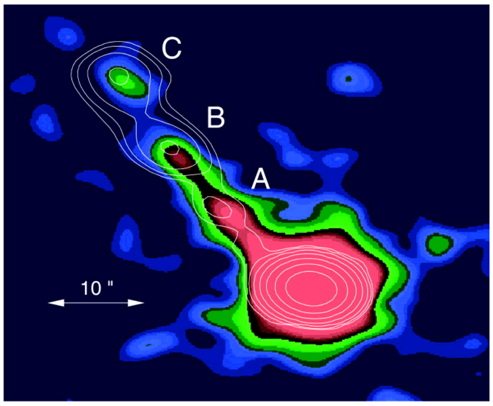

Figure 9: Figure 7a of Siemiginowska et al. [33] shows the X-ray peak intensities, (color image), well upstream of each radio peak, (contours), with which they seem to be identified.

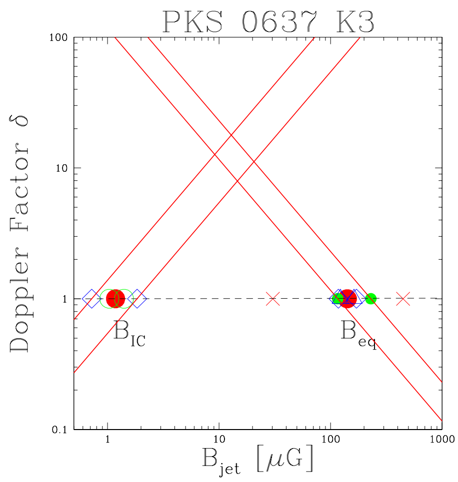

Figure 10: Calculation of the magnetic field and effective Doppler factor, and their uncertainties (see text for details).

4. JET PROPERTIES

We will make the usual assumption of a minimum energy condition, which is very nearly that in which the energy density in the magnetic field equals that in relativistic particles [34]. This breaks the degeneracy between the product of the particle density and magnetic field strength which enters the calculation of the observed synchrotron flux density. Adopting this assumption, and also assuming that the X-rays arise from inverse Compton scattering on the cosmic microwave background, allows one to calculate the magnetic field in the jet frame, and also the effective Doppler factor $\delta = [\Gamma(1-\beta\cos\theta)]^{-1}$ where Γ is the bulk Lorentz factor of the jet, and θ is its direction of motion relative to our line of sight, according to the formalism of Tavecchio et al. [25]. We do not generally know the direction of the jet, so we assume $\delta = \Gamma$, since 2Γ is the maximum value of δ for very large Γ and θ=0.

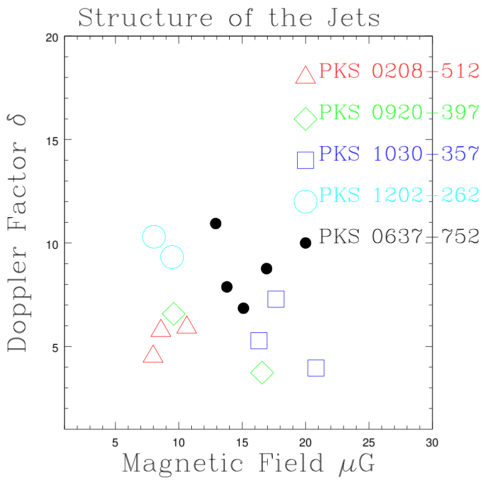

Figure 11: Estimate of the jet Doppler factor and rest frame magnetic field for the five jets labeled. Multiple spatially resolved regions of the same jet are indicated with the same shape symbols.

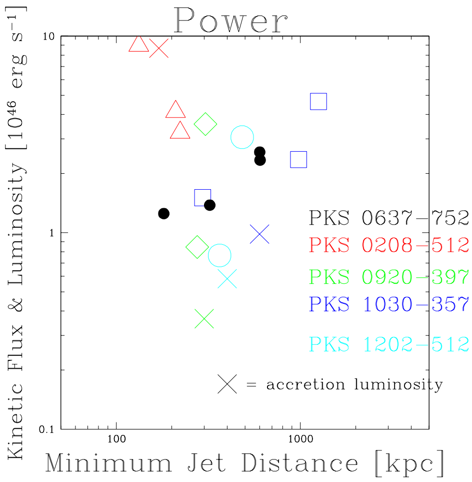

Figure 12: Kinetic power carried through each of the jet regions shown in Fig. 11, with the same symbols for the different quasars. The crosses estimate the total radiative luminosities of the quasars.

4.1. Magnetic Field and Doppler Factor

Figure 10 illustrates this calculation. The largest solid dots are independent calculations which assume the jet velocity is non-relativistic with respect to the cosmic microwave background frame; i.e., $\delta = 1$. Using standard equipartition assumptions for the radio emission, we derive the magnetic field B_{eq} of about 120 μG. If we assume instead that the X-rays arise from IC/CMB from an extrapolation of the same electrons giving the radio synchrotron emission, we derive the contradictory result that the magnetic field B_{IC} must be about 1.5 μG. This discrepancy can be resolved if we assume the jet is in bulk relativistic motion with Lorentz factor Γ. In that case the magnetic field B in the jet frame transforms inversely with δ as $B = B_{eq}/\delta$ and directly as $B = B_{IC} \times \delta$, so that we are guaranteed a solution for B and δ. For the particular region around 8.3$''$ along the jet of PKS 0637-752 shown in Figure 10, we find $B = 10.3\mu$G and $\delta = 10.5$.

The additional symbols along the $\delta = 1$ line in Figure 10 illustrate the uncertainty in that determination. These are dominated by the systematic errors of our assumptions: a spectral index change of $\pm$ 0.2 of the radio emission (diamonds), the case that the proton energy density is k=0 or k=10 times that of the electrons rather than k=1 as assumed (small dots); a total energy density a factor of ten greater than minimum (crosses). We also show the Poisson error in the X-ray flux (open circles), which typically is considerable since we divide into spatial regions of only 10 to 30 counts.

In Figure 11 we show the resulting B and δ values for two to four regions in five different quasar jets (cf. Figure 2). We typically measure fields 5 to 25 μGauss and Doppler factors 3 to 12. When we apply the systematic error considerations independently to each region, we cannot exclude a single magnetic field value and Doppler factor for the entire jet length. However, it is intriguing to speculate that the systematic deviations apply uniformly along the jet so that we are detecting differences among the regions.

4.2. Kinetic Flux

In Figure 12 we calculate the flux of kinetic energy carried along the jet. This is given by

$$K = \Gamma^2 \pi r^2 \beta c U, \tag{5}$$

where U is the total internal energy density, the sum of the densities in particles and magnetic field, and $U = \frac{B^2}{8\pi}(2 + k)$ under our equipartition assumptions. This shows that the lines $(B\,\Gamma)^2 = (B\,\delta)^2$ give constant kinetic flux. Since the radiative efficiency of the jet is so small, the Kinetic flux is probably constant where we see the jet, and the true (B,δ) values for each region of a given jet probably fall along a line of constant $B\delta$. (This might fail where the jet is mechanically interacting with an external medium, as manifested by a radio lobe or change in angle to the line of sight.)

Taking $\Gamma = \delta$, we can see that the maximum value of the angle to our line of sight is given by $\cos(\theta_{max}) = (\delta - 1/\delta)/\sqrt{(\delta^2 - 1)}$. We use this angle to de-project the jets and plot the minimum distance from the quasar for each specific region. The kinetic flux values are large, of order 10^{46-47} erg cm^{-2}s^{-1}. We have assumed the ratio of proton to electron energy density is k=1. If k=0 the kinetic power is about 3 times less, While if k=10 the power is about 20 times higher.

In any case the kinetic power is comparable to or larger than the accretion luminosity of the quasar cores. This means it represents a significant, or even a dominant portion of the accretion energy budget. Thus jet production must be considered as part of any complete accretion theory, as has been pointed out previously [17].

4.3. Is the Emission Really Inverse Compton Scattering?

Whether an electron primarily radiates via the synchrotron or the inverse Compton mechanism depends on whether the magnetic field energy density, $B^2/(8\pi)$, or the CMB energy density, $a\Gamma^2 T_0^4(1+z)^4$, is greater. More precisely, the fractional radiation into each channel is the ratio of each energy density to the sum of the two energy densities. The solid line in Figure 13 indicates this dividing line as a function of magnetic field and redshift, in a frame which is at rest with respect the CMB. We plot magnetic fields deduced for various regions of jets which are observed in X-rays, from the surveys of Marshall et al. [15] and Sambruna et al. [14, 35]. The crosses are calculated using only the radio data, assuming equipartition and that there is no Doppler beaming, δ=1. If all those assumptions were true, then synchrotron radiation would be the primary contributor to the X-ray emission, as it is for the radio and optical. Note that even in this case, a sizeable group of the jets which have B$\leq$60μG would be emitting X-rays via IC/CMB if they were actually at redshift z=3. At that time, their IC/CMB X-ray surface brightness would be the same as their current IC/CMB X-ray brightness, which is the square of the ratio of B on the solid line at their current redshift, to the B given by the "x" symbol.

The above is a very pessimistic picture of IC/CMB radiation, because there is substantial evidence that these powerful FRII jets are moving with significant bulk Lorentz factors. This enhances the CMB energy density as seen in the jet rest frame by a factor Γ^2 [36]. For example, the magnetic field would need to be larger than that given by the dashed line, in order that a jet moving with Γ=5 emit primarily via synchrotron radiation.

To explain the X-ray emission by IC/CMB we generally need to invoke relativistic beaming, as originally pointed out for PKS 0637-752 [25, 26]. The resulting fields are shown by the triangle points in Figure 13.

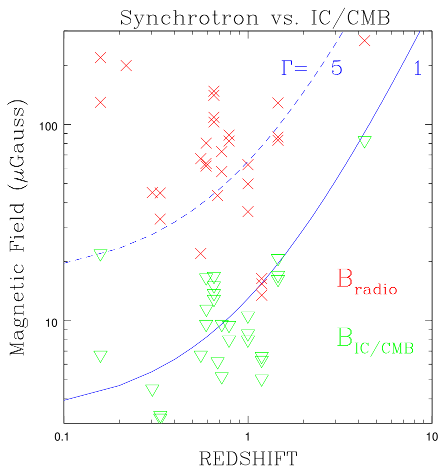

Figure 13: Crosses plot magnetic fields calculated solely from radio observations and minimum energy considerations. The triangles calculate the magnetic fields for the same jets assuming that the X-rays are produced by IC/CMB. The solid line shows the minimum magnetic field required to equal the energy density of the CMB as a function of redshift. The dashed line shows the (larger) field which is required if the jet is in relativistic motion with Lorentz factor Γ=5.

5. X-RAY JETS AT LARGE REDSHIFT

Where *are* all the bright X-ray jets at large redshifts? They must be among tens of thousands of unidentified *ROSAT* sources, and also among *ROSAT*, *ASCA*, and *Einstein* quasar identifications. None of those facilities could distinguish the kinds of jets we are observing from a point source, nor resolve them from a quasar 10 to 20 arcsec away and of much greater brightness (cf. Figure 1). They may even be among the extreme X-ray/Optical ratio sources discovered by Koekemoer et al. [37] in the *Chandra* deep surveys.

ROSAT, *ASCA*, and *Einstein* all studied the bright radio loud quasar GB 1508+5714, at redshift z=4.3. The *Chandra* image showed that this quasar was not point-like [38], and Siemiginowska et al. [39], in conjunction with radio data presented by Cheung [40], showed that it was an X-ray jet. At this conference Cheung [41] has presented evidence of radio and X-ray jets in the quasar 1745+624=4C +62.29 at redshift z=3.889.

As noted by Schwartz [18] there could, and therefore should, be radio quiet X-ray jets. This is because the lower energy electrons emitting the X-rays have longer lifetimes than the electrons emitting $\approx$10 MeV γ-rays, which electrons incidentally emit the observed GHz radio emission. So far such a radio quiet jet has not been found.

To confidently establish the actual occurrence of the IC/CMB mechanism, we should observe that jets at redshifts beyond z=1 have a markedly higher ratio of X-ray to radio flux. Figure 14 plots X-ray jet to radio jet, and X-ray jet to radio core ratios. The solid line with Γ = 7 is scaled to the parameters fit to explain the PKS 0637-752 jet, showing the predicted increase in X-ray to radio ratio with redshift. The other solid

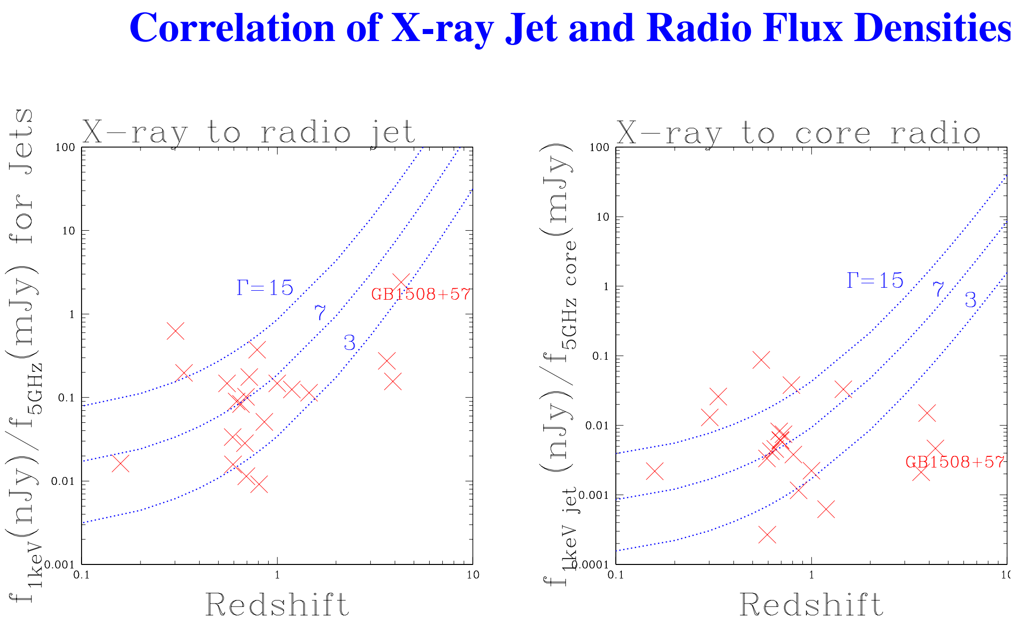

Figure 14: Left panel plots the ratio of X-ray to radio flux density observed in jets, vs. their redshift. The solid lines predict how this ratio would increase if the same objects were moved to higher redshifts, for the cases of Γ=3, 7, and 15. The right panel plots the X-ray jet to radio core flux ratio.

lines show different values of Γ, but are assumed to have the same magnetic field and relativistic particle population as PKS 0637-752. Appropriate observations have not yet been done which might detect this increase. Among the various jets there is naturally a dispersion in the intrinsic properties, and the relatively short 5 and 10 ks *Chandra* observations will naturally pick out objects with larger f_x/f_r ratios due to selection effects. These are essentially all the observations for $z \leq 2$. In contrast, all the jets for $z \geq 3$ result from serendipitous observations of high redshift quasars, so we might naturally expect the more numerous objects with smaller Γ factors to appear more frequently. A more critical assessment awaits *Chandra* observations of high redshift quasars selected by their flat spectrum radio core, as was done in the Marshall et al. [15] survey, and proper statistical use of the X-ray upper limits.

6. CONCLUSIONS

X-rays dominate the power radiated by powerful AGN jets. Study of the spectral energy distribution from the radio through optical and into the X-ray band potentially gives us information on the acceleration sites, via changing ratios of the X-ray to radio flux density; the deceleration of the bulk motion of the jet; and the hadron content of the jet. With the assumption of equipartition conditions, we have estimated typical Lorentz factors of 3 to 12 and magnetic fields of 5 to 25 μG in order for the X-ray emission to be produced by inverse Compton scattering on the cosmic microwave background.

The kinetic fluxes of the jets are in excess of 10^{46} and sometimes 10^{47} ergs cm^{-2}s^{-1}. Since this is the same order or greater than the radiative luminosity of their parent quasar, we can speculate that the jets provide a mechanism to greatly exceed the Eddington accretion rate. This might be significant for the rapid growth of massive black holes in the early universe. These kinetic fluxes are also sufficiently large to power the cavities in X-ray clusters and stop cooling flows. Although the occurrence in a cluster obviously greatly changes the appearance of the radio source, central cluster galaxies have black hole masses similar to quasars, and it is plausible that their jets are also intrinsically as powerful.

In the case that jets emit X-rays via the IC/CMB mechanism, then for given jet parameters, the X-ray surface brightness will remain constant to whatever large redshift such a jet might exist. For the jets we already observe at redshifts ≈ 0.5 to 1, even if they are not relativistic and not emitting via IC/CMB, their equipartition magnetic field is small enough that IC/CMB must dominate when similar jets are at redshifts greater than ≈ 2 to 3. Thus X-rays may be a natural channel to search for the earliest activity in the universe.

Acknowledgments

This research was supported in part by NASA contract NAS8-39073 to the *Chandra* X-ray Center. I have benefited by working on a jet survey with M. Birkinshaw, J. Gelbord, D. Jauncey, J. E. J. Lovell, H. L. Marshall, D. Murphy, E. Perlman, and D. M. Worrall. I thank the organizers for a very stimulating 22nd Texas Symposium.

References

[1] Weisskopf, M.C., Tananbaum, H. D., Van Speybroeck, L.P., & O'Dell, S.L. 2000, Proc. SPIE, 4012, 2
[2] Feigelson, E. D. 1980, PhD Thesis, Harvard Univ.
[3] Feigelson, E. D., et al. 1981, Ap. J. 251, 31
[4] Schreier, E. J., Gorenstein, P., & Feigelson, E. D. 1982, Ap. J., 261, 42
[5] Willingale, R. 1981, MNRAS, 194, 359
[6] Harris, D. E., & Stern, C. P. 1987, Ap. J., 313, 136
[7] Yang, Y., Wilson, A. S., & Ferruit, P. 2001, ApJ 563, 124.
[8] Fabian, A. C., et al., 2000, MNRAS, 318, L65.
[9] Heinz, S., Choi, Y.-Y., Reynolds, C. S., & Begelman, M. C. 2002, ApJ., 569, L79
[10] Wilson, A. S., Young, A. J., & Shopbell, P. L. 2000, ApJ, 544, L27
[11] Hardcastle, M. J., Birkinshaw, M., & Worrall, D. M. 2001, MNRAS, 323, L17
[12] Birkinshaw, M., Worrall, D. M., & Hardcastle, M. J. 2002, MNRAS, 335, 142
[13] Worrall, D. M., Hardcastle, M. J., & Birkinshaw, M. 2001, MNRAS, 326 L7
[14] Sambruna, R. M., Maraschi,L., Tavecchio, F., Urry, C. M., Cheung, C. C., Chartas, G., Scarpa,R., & Gambill, J. K. 2002, ApJ, 571, 206
[15] Marshall, H. L., Schwartz, D. A., Lovell, J. E. J., Murphy, D. W., Worrall, D. M., Birkinshaw, M., Gelbord, J. M., Perlman, E. S., & Jauncey, D. L. 2005, ApJS, 156, 13
[16] Rees, M. J. 1971, Nature, 229, 312
[17] Meier, D. L. 2003, NewAR, 47, 667
[18] Schwartz, D. A. 2002, ApJ, 569, L23
[19] Dermer, C. D., & Atoyan, A. M. 2002, ApJ 568, L81
[20] Stawarz, L., & Ostrowski, M. 2002, ApJ, 578, 763
[21] Stawarz, L., Sikora, M., Ostrowski, M., & Begelman, M. C. 2004, ApJ, 608, 95
[22] Schwartz, D. A. et al. 2000, ApJ, 540, L69
[23] Chartas, G. et al. 2000, ApJ, 542, 655
[24] Schwartz, D. A. et al. 2001, ASP Conf. Proc. 234, "X-ray Astronomy 2000," R. Giacconi, S. Serio, L. Stella, eds., 493
[25] Tavecchio, F., Maraschi,L., Sambruna, R. M., & Urry, C. M. 2000, ApJ, 544, L23
[26] Celotti, A., Ghisellini, G., & Chiaberge, M. 2001, MNRAS, 321, L1
[27] Miller, B. P. 2002, Undergraduate Thesis, MIT.
[28] Mueller, M. & Schwartz, D. A. 2005, in preparation.
[29] Marshall, H. L. et al. 2001, ApJ, 549, 167
[30] Bahcall, J. N. et al. 1995, ApJ, 452, L91
[31] Felten, J. E. & Morrison, P. 1966, ApJ, 146, 686
[32] Fixsen, D. J., Cheng, E. S., Gales, J. M., Mather, J. C., Shafer, R. A., & Wright, E. L. 1996, ApJ, 473, 576
[33] Siemiginowska, A. et al. 2002, ApJ, 570, 543
[34] Miley, G. 1980, ARAA, 18, 165
[35] Sambruna, R. M. et al. 2004, ApJ, 608, 698
[36] Dermer, C. D. & Schlickeiser, R. 1994, ApJS, 90, 945
[37] Koekemoer, A. M. et al. 2004, ApJ, 600 L123
[38] Yuan, W., Fabian, A. C., Celotti, A., & Jonker, P. G. 2003, MNRAS, 346, L7
[39] Siemiginowska, A. et al. 2003, ApJ, 598, L15
[40] Cheung, C. C. 2004, ApJ, 600, L23
[41] Cheung, C. C., Wardle, J. F. C., & Lee, N. P. 2005, in *Proceedings of the 22nd Texas Symposium, Palo Alto, 2004* edited by P. Chen, eConf C04xxxx, 1613